Bronze Wool as a Porous Mixer for Air Temperature Uniformity in Energy Exchangers

Amirreza Mahmoudi[1*], Melanie Fauchoux[1], Carey Simonson[1]

[1]Department of Mechanical Engineering, University of Saskatchewan, Saskatoon, Saskatchewan, Canada

[*]Corresponding author; email: yhm570@usask.ca

Preprint (author's original). Submitted to* the Transactions of the Canadian Society for Mechanical Engineering (TCSME)*; under review (2025).

Abstract

This study investigates the use of bronze wool as a porous air mixer to improve temperature uniformity at the outlet of a liquid-to-air membrane energy exchanger (LAMEE). Traditional air mixers often cause excessive pressure losses and are difficult to install in compact systems. Bronze wool offers a lightweight, space-efficient alternative with favorable thermal and structural properties. Experimental evaluations were conducted using mixers with varying wool mass, porosity, and structure, under both horizontal and vertical duct orientations. Results show that bronze wool mixers significantly reduce temperature gradients, achieving up to 75% statistical effectiveness in horizontal ducts and 54% range effectiveness in vertical ducts. In compact wool structures, thermal conduction within the metal fibers is the primary temperature homogenization mechanism, while physical mixing from advection and dispersion occurs in higher-porosity structures. Among all configurations, the accordion wool structure demonstrated the highest range effectiveness, attributed to enhanced multi-directional conduction. The pressure drop across the mixers remained relatively low, confirming the suitability of metal wool air mixers for use in systems where minimizing flow resistance is critical. The findings demonstrate that bronze wool mixers provide a compact, low-resistance, and effective solution for temperature homogenization in air ducts.

K**eywords:**

Air Mixing; Porous Mixer; Bronze Wool; Temperature Uniformity; Liquid-to-air Membrane Energy Exchanger (LAMEE).

Nomenclature

Symbol	Description	Unit
Acronyms		
ASHRAE	American Society of Heating, Refrigerating and Air-conditioning Engineers	-
CFD	Computational fluid dynamics	-
LAMEE	liquid-to-air membrane energy exchanger	-
Latin symbols		
m	bronze wool mass	g
ΔP	pressure drop	Pa
Q	volume flow rate	l/min
$R_{\mathrm{cs},T}$	range of the temperatures measured at different locations across the duct cross-section	˚C
R_{t}	range (difference between the maximum and minimum) of several measurements conducted over a given time period	measurand unit
Re	Reynolds number	-
RH	relative humidity	%
T	temperature	˚C
U	uncertainty at 95% confidence level	measurand unit
Greek symbols		
ε	porosity	-
η_{r}	range mixing effectiveness	-
η_{s}	statistical mixing effectiveness	-
ρ	density	kg/m^3
$\sigma_{\mathrm{cs},T}$	standard deviation of the temperatures measured at different locations across the duct cross-section	˚C
σ_{t}	standard deviation of several measurements conducted over a given time period	measurand unit
Subscripts		
a	air	-
amb	ambient	-
d	downstream	-
i	inlet	-
LD	liquid desiccant	-
max	maximum	-
min	minimum	-
mixer	across the air mixer	-
orifice	across the orifice plate	-
o	outlet	-
u	upstream	-

1. Introduction

Air mixing in duct systems is a pivotal process in various industrial and environmental applications, playing a crucial role in achieving uniform distribution of properties. This uniformity is crucial for precise control and measurement in numerous mechanical and thermal systems. In Heating, Ventilation, and Air Conditioning (HVAC) systems, temperature is a prominent parameter, and a uniform temperature profile is required where a point measurement method is used to acquire the mean value of flow temperature. Previous researchers have investigated several mixing methods, but achieving high mixing effectiveness, especially in intricate or constrained environments, remains challenging.

Air mixing techniques have primarily focused on mechanical mixers and intricate flow geometries, yet these solutions often introduce complexity or increase energy consumption. The performance of air mixers is quantified using mixing effectiveness, which can be calculated by comparing the uniformity of the temperature profile upstream and downstream of the mixer. The National Bureau of Standards (now known as NIST) pioneered testing static air mixers and reported the performance of various orifice and louver air mixers (Faison et al., 1970, 1967). The results showed that orifice mixers can only provide a high mixing effectiveness at the cost of high pressure drops; therefore, the louver mixers are the preferred choice in most applications. These findings have been supported by a recent research project by the American Society of Heating, Refrigerating, and Air-Conditioning Engineers (ASHRAE) investigating louver, louver-baffle, orifice, and orifice-target mixers (Ahmed et al., 2020). The results of the CFD study showed that, depending on the louver angle, a louver air mixer has an effectiveness ranging from 75% to 85% at a distance of 1.5 hydraulic diameters downstream of the mixer. The observations showed that static air mixers act by adding turbulence to the air stream.

The concept of using porous media for mixing and homogenization has been explored in different contexts. It has been shown that porous media can enhance the homogeneity of temperature fields in fluid flows and reduce the amplitude of the oscillations if the heat source is transient (Li et al., 2023). The lower the porosity of the media, the higher the enhancement of heat transfer rates and the more uniform the temperature fields. The conductivity of the material has a direct relationship with the dampening effect on the thermal fluctuations. As a supporting example from a different context (mixing fronts of two different fluids), Rousseau et al. (2023) showed that porous media can be effective mixers, and dispersion is the dominant mixing mechanism in packed beds.

However, the application of porous media in air temperature profile uniformization is relatively unexplored. A literature survey has shown that no previous research has used metal wool as an air mixer. This gap presents a unique opportunity to contribute to the field, particularly in applications where precise temperature measurement is critical but space or structural restrictions do not allow application of traditional mixers. This study introduces a novel approach that leverages the inherent properties of metal wool, specifically bronze wool, as a porous medium for air mixing within duct systems. The use of metal wool, a material traditionally overlooked in air mixing applications, offers a unique blend of porosity, thermal conductivity, and structural flexibility, potentially overcoming the limitations of conventional methods.

In this paper, an experimental study is presented where bronze wool is used as an air mixer to homogenize the temperature profile in a duct. This work is a part of a research project on heat and mass transfer in liquid-to-air energy exchangers (LAMEEs) (Fauchoux et al., 2025), where heat transfer between air and liquid-desiccant creates a temperature gradient in the air duct downstream of the LAMEE. The primary objective is to improve the uniformity of the air temperature profile at the outlet of the LAMEE, allowing for accurate

bulk temperature measurement. A simple method of making a metal wool air mixer is introduced, and the mechanisms that lead to the homogenization of the temperature are discussed. The effectiveness of this mixing solution will be quantified by measuring the temperature profile and calculating the mixing effectiveness for various bronze wool porosities and structures, as well as different duct orientations. The results contribute to the understanding of thermally conductive porous media in air mixing applications and offer a practical and efficient solution for systems where temperature uniformity is crucial, but there are limitations for installation or pressure loss of the mixer, including the lab-scale studies of energy exchangers.

2. Methodology

The experimental setup, shown schematically in Figure 1, is designed and primarily used for research on frosting in LAMEEs. In this setup, air passes through a flat-plate, counter-crossflow energy exchanger, where a vapor-permeable membrane acts as the heat and moisture transfer surface between air and a colder liquid desiccant. The liquid flow rate is selected to be sufficiently high to ensure that liquid temperature remains constant across the exchanger. This uniform liquid temperature helps maintain a relatively uniform surface temperature distribution. The operating conditions are presented in Table 1.

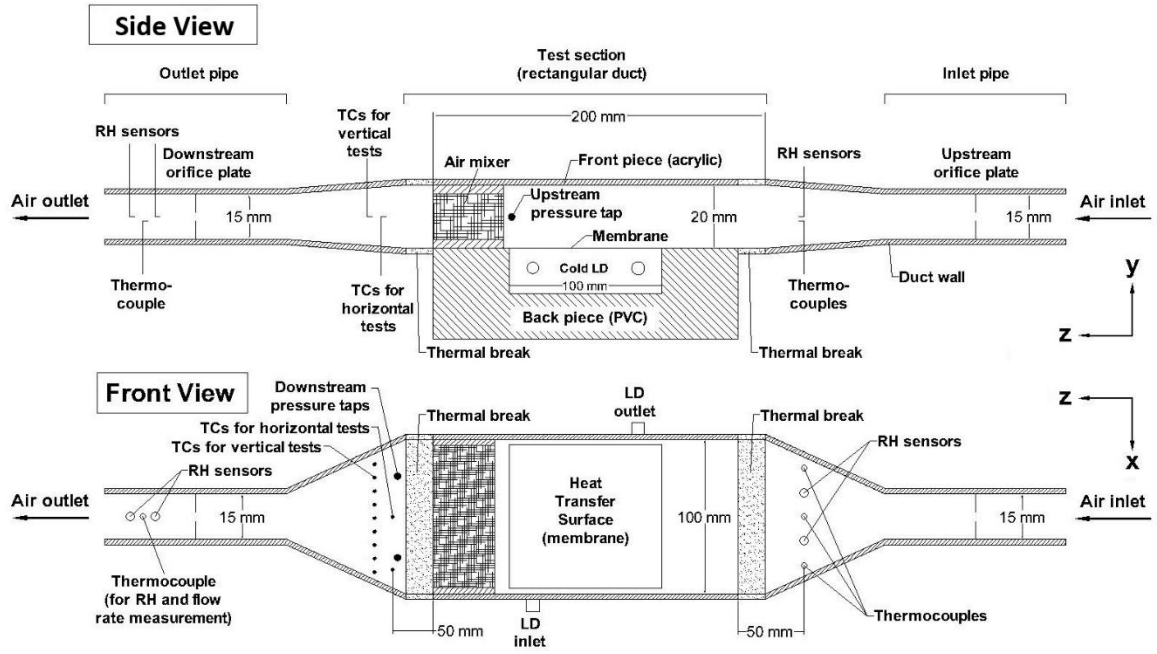

Figure 1. Schematic of the test section (not-to-scale), showing main dimensions and sensor locations.

Table 1. Temperature and flow rate operating conditions.

Location	Flow rate, Q (l/min)	Temperature, T (°C)
Air inlet	9.0 ± 0.3	10.0 ± 0.2
Liquid inlet	0.200 ± 0.030	0.0 ± 0.2
Ambient	-	0.0 ± 0.2

It is necessary to know the mean air temperatures upstream and downstream of the LAMEE to be able to evaluate the effectiveness of the energy exchanger with reasonable accuracy. While the air temperature profile is uniform at the inlet, significant gradients exist in the outlet profile due to the heat transfer occurring in the energy exchanger. Therefore, the metal wool air mixer is installed in the outlet of the LAMEE to homogenize the temperature profile and allow for accurate evaluation of the mean air temperature at the outlet of the LAMEE with a limited number of sensors.

The entire test setup is installed inside an environmental chamber, which produces the conditioned air. Airflow is generated using a regenerative fan and controlled using a variable-frequency drive (VFD) controller. The test section is thermally insulated to minimize heat gains from the ambient environment.

2.1. Instrumentation and measurements

Temperature measurements are conducted using type T thermocouples calibrated with a Hart Scientific 9105 dry well calibrator. The readings are conducted automatically using an electronic data acquisition module. The mounting system of the thermocouples, which are shown as TC in Figure 1, allows for positioning them at different points along the width of the duct. The full temperature grid is generated by compiling measurements with the same thermocouples at different locations along the width of the duct.

The effectiveness of the bronze wool air mixer is evaluated with the LAMEE in both horizontal and vertical orientations (Figure 2). When the LAMEE and the duct are oriented horizontally (Figure 2(a)), air flows over the horizontal cold surface, and forced convection is the dominant heat transfer mechanism. Based on previous experience with temperature measurement in LAMEEs, a symmetric temperature profile is expected under these conditions, with negligible gradients along the horizontal dimension of the duct cross-section (x direction in Figure 2(a)) (Fauchoux et al., 2025). Therefore, the temperature profile is captured in half of the duct cross section, using two temperature measurements conducted at two locations along the x direction. One thermocouple is installed at the centerline, and the other is closer to the side wall of the duct. Both thermocouples are located two centimeters downstream of the mixer, equal to about half of the hydraulic diameter of the duct. When the LAMEE (and the duct) is oriented vertically (Figure 2(b)), the vertical cold surface promotes natural convection (Fauchoux et al., 2025), which can cause significant temperature gradients and an asymmetric profile in the vertical (y) direction. Therefore, the temperature profile is captured in the full cross section of the duct, using nine thermocouples, equally spaced along the x direction. This thermocouple configuration improves the resolution of the measurement grid in the vertical direction and captures any asymmetry in the temperature profile that can occur due to natural convection.

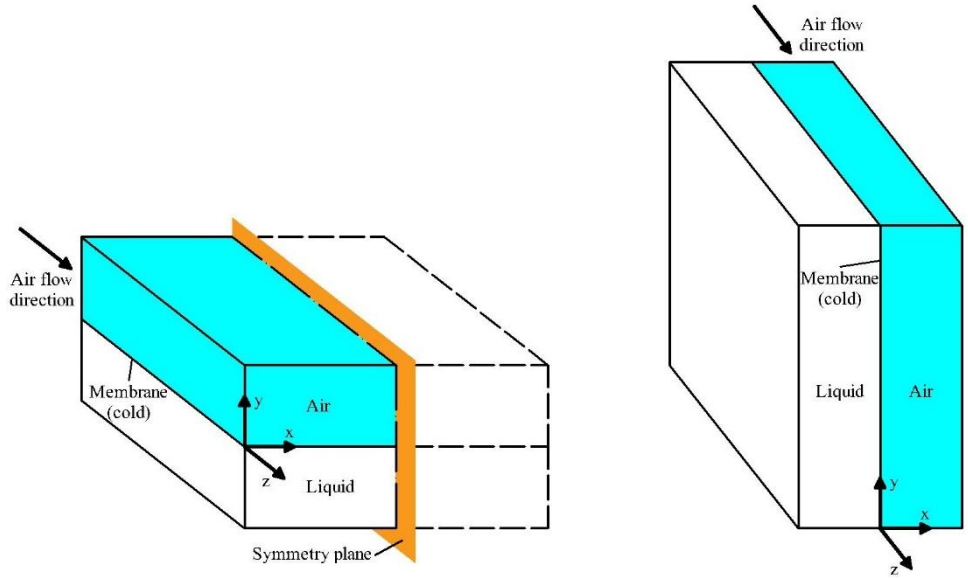

Figure 2. Schematic of the LAMEE, showing the liquid channel, air channel and the membrane in (a) horizontal, and (b) vertical orientation. For the horizontal orientation, the plane of symmetry and the half-duct used in the temperature profiles in this paper are shown.

The air flow rate is measured using orifice plates located upstream and downstream of the test section. The Reynolds number is then calculated based on the measured flow rate and air density, with the latter evaluated using the ideal gas law and the measured air temperature. Comparing the upstream and downstream flow rates confirmed that air leakage was negligible and that mass balance was maintained throughout the tests. The acceptability of mass conservation, energy balance, and inlet and outlet conditions was checked and verified based on the applicable guidelines in ASHRAE Standard 84 (ASHRAE, 2020). To achieve accurate and reliable flow rate measurements, the orifice plates were sized, manufactured, and installed in accordance with the guidelines provided in (ISO, 2003; Reader-Harris, 2015). Validyne P17 pressure transducers with full-scale readings of 1500 and 3500 Pa are used to measure pressure differentials across the orifice plates. A Validyne DP103 with a full-scale reading of 350 Pa is used to measure the pressure drop across the air mixer.

Air relative humidity (RH) is measured as the average of the readings of two sensors in the inlet and two sensors in the outlet. Air relative humidity is monitored as part of the steady-state criteria, which will be discussed in the steady-state conditions section.

2.2. Calibration and uncertainty

All sensors were calibrated across their intended measurement ranges using laboratory standards and in accordance with recognized best practices. Multi-point calibration was performed on the thermocouples and pressure transducers using a Hart Scientific dry-well thermocouple calibrator and a Druck DPI-650 precision pressure calibrator, respectively. The RH sensors are calibrated using humidity fixed-point method, following the guidelines of ASTM E104 (ASTM, 2020). Details of the calibration instruments and procedures are presented in Table 2.

Table 2. Measurement instrument calibration: ranges and methods

Equipment	Model	Calibration range	Calibration method/instrument
Thermocouples	T-Type, gauge 24	0 to 25˚C	Hart Scientific 9105 Drywell Calibrator
RH sensors	Honeywell HIH 4020	10 to 90%RH at 25˚C	Humidity fixed point method using aqueous salt solutions; temperature compensation using the manufacturer's recommended correlation.
Differential pressure transducers	Validyne P17 and DP103	0 to 350 Pa / 3500 Pa	Druck DPI 650 Precision Pressure Calibrator
Liquid flow rate meter (pump feature)	FPU500 OMEGAFLEX peristaltic pump	50 and 530 ml/min	The ml/rpm of pumping rate was calibrated manually, using the timed volumetric method.

The accuracy of each measurement was evaluated using the standard uncertainty analysis method provided by ASME PTC 19.1 (ASME, 2019). The overall standard uncertainty consists of random and systematic errors. Random uncertainty calculations involve the evaluation of the standard deviation of the repeated measurements and get more accurate with increasing number of measurements. Systematic uncertainties can stem from various other errors, including sensor bias and data reduction accuracy.

Table 3 summarizes the uncertainties in the measured and calculated parameters. All standard uncertainties reported here are at a confidence level of 95%. The relatively high uncertainties in the calculation of range effectiveness, i.e. ±16% effectiveness and ±11%

effectiveness for the horizontal and vertical orientations, respectively, are attributed to the limited temperature range across the duct cross-section ($R_{\mathrm{cs},T}$). $R_{\mathrm{cs},T}$ depends on the operating conditions of the LAMEE and could be increased by raising the temperature difference between the air and liquid streams. However, this study focuses on evaluating the performance of the metal wool air mixer in a LAMEE operating with 10˚C temperature difference, which reflects the average condition anticipated in the experimental research that motivated this work.

Table 3. Uncertainties in the measured and calculated parameters

Parameter	Type	Uncertainty
Temperature, T (air inlet and liquid temperatures)	Measured	±0.2˚C
Temperature, T (air mixer temperature grid)	Measured	±0.1˚C
Relative humidity, RH	Measured	±5.2% RH
Air mixer differential pressure, ΔP_{mixer}	Measured	±2.0 Pa
Orifice plates differential pressure, $\Delta P_{orifice}$	Measured	±35 Pa
Air volume flow rate, Q_{a}	Calculated	±3.5% of the value
Air Reynolds number, Re_a	Calculated	±3.5% of the value
Range effectiveness, η_{r} (with horizontal duct orientation)	Calculated	±16% effectiveness
Range effectiveness, η_{r} (with vertical duct orientation)	Calculated	±11% effectiveness
Statistical effectiveness, η_{s} (with horizontal duct orientation)	Calculated	±8% effectiveness
Statistical effectiveness, η_{s} (with vertical duct orientation)	Calculated	±5% effectiveness

2.3. Steady-state conditions

In each individual test, the system was allowed to reach steady-state conditions before temperatures were recorded. To verify steady-state conditions, the variations of the inlet and outlet conditions were evaluated relative to their respective measurement uncertainties. At each time step during the test, two categories of steady-state indicators (Table 4) were checked: (a) the difference between the maximum and minimum of the inlet conditions recorded over the last hour, and (b) the standard deviation of both inlet and outlet conditions over the last hour. Steady state was considered established when all conditions from both categories were satisfied concurrently. When the temperature measurements were completed at one location, the thermocouples were moved to the next location across the width of the duct to conduct the next test.

Table 4. Indicators used to determine steady-state conditions during the experiments.

(a) Indicators based on the range of the measured parameter	
$R_{\mathrm{t},T_{\mathrm{a,i}}} < U_{T_{\mathrm{a}}}$;	
$R_{\mathrm{t},T_{\mathrm{LD,i}}} < U_{T_{\mathrm{LD}}}$;	
$R_{\mathrm{t},RH_{\mathrm{a,i}}} < U_{RH_{\mathrm{a}}}$;	
(b) Indicators based on the standard deviation of the measured parameter	
$2 \times \sigma_{\mathrm{t},T_{\mathrm{a,i}}} < U_{T_{\mathrm{a}}}$;	$2 \times \sigma_{\mathrm{t},T_{\mathrm{a,o}}} < U_{T_{\mathrm{a}}}$;
$2 \times \sigma_{\mathrm{t},T_{\mathrm{LD,i}}} < U_{T_{\mathrm{LD}}}$;	$2 \times \sigma_{\mathrm{t},T_{\mathrm{LD,o}}} < U_{T_{\mathrm{LD}}}$;
$2 \times \sigma_{\mathrm{t},RH_{\mathrm{a,i}}} < U_{RH_{\mathrm{a}}}$;	$2 \times \sigma_{\mathrm{t},RH_{\mathrm{a,o}}} < U_{RH_{\mathrm{a}}}$;

2.4. Bronze wool air mixer

The bronze wool is installed in a cassette-like enclosure made of 2-mm thick acrylic sheets before being inserted into the test section. The cassette, its dimensions, and a magnified image of the wool texture are presented in Figure 3. The different wool structures studied in this paper are shown in Figure 4. If the inside space of the cassette is occupied with one piece of non-modified metal wool, the fibrous structure is considered “basic” (Figure 4(a)). If the piece of wool is squeezed in a way that the metal fibers are rearranged mainly in one direction (Figure 4(b)), the wool structure is termed “directional.” In “spiral” structure (Figure 4(c)), the cassette is filled with one or more pieces of wool rolled to form a spiral shape. In “accordion” structure, the metal wool is folded to form an accordion-like structure.

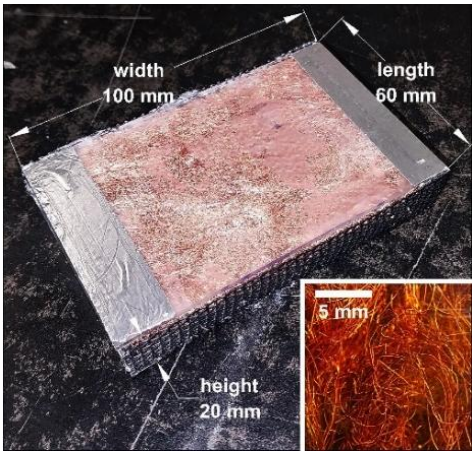

Figure 3. The metal wool air mixer (inset: a magnified view of the wool)

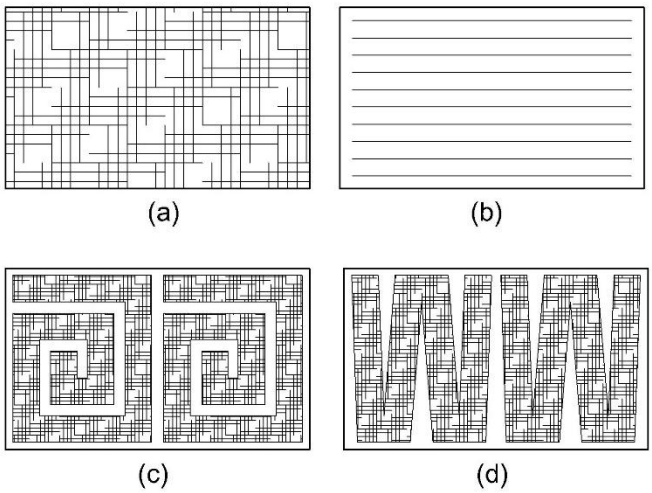

Figure 4. Wool structures: (a) Basic structure; (b) directional structure; (c) spiral structure; and (d) accordion structure. Air flow direction is from side to side in these schematics.

The compactness of metal wool is expected to influence mixing effectiveness through improving heat conduction. The compactness of metal wool has an inverse relation with its porosity, which quantifies the amount of void space inside the mixer. Eq. (1) can be used to calculate the porosity of the metal wool mixer.

$$\varepsilon = 1 - \frac{\rho_{wool}}{\rho_{bronze}} \quad (1)$$

where ε is the porosity of the mixer medium, ρ_{wool} is the effective density of the bronze wool piece when fitted into the cassette, and ρ_{bronze} is the density of bronze. The internal volume of the cassette is 8.28×10^{-5} m^3, and the density of bronze is 8800 kg/m^3 (Bergman et al., 2017). ρ_{wool} can be calculated based on the measured mass of the bronze wool and the internal volume of the cassette, which is occupied by the piece of wool. Table 5 summarizes the characteristics of the mixer in different cases, including mass, porosity, and structure of the metal wool. As will be shown later in this paper, the relatively high porosity of the bronze wool air mixer helps maintain acceptable mixing effectiveness while keeping the pressure loss relatively low.

198 Table 5. Mass, density, and porosity of the metal wool in different experiments.

Case #	Designation	Orientation	Mixer	Wool mass (g)	Wool porosity	Structure
1	No Mixer (H)	Horizontal	No	-	-	-
2	Basic (H98)	Horizontal	Yes	16.5	98%	 Basic
3	No Mixer (V)	Vertical	No	-	-	-
4	Basic (V99)	Vertical	Yes	6.4	99%	 Basic
5	Directional (V97)	Vertical	Yes	23.4	97%	 Directional
6	Spiral (V97)	Vertical	Yes	23.4	97%	 Spiral
7	Accordion (V97)	Vertical	Yes	23.4	97%	 Accordion

199 **2.5. Mixing effectiveness**

200 In HVAC applications, the two primary methods for evaluating mixing effectiveness
201 are range effectiveness and statistical effectiveness (Robinson, 1997). Range effectiveness,
202 η_{r}, is determined by measuring the temperature range upstream and downstream of the mixer
203 and applying Eq. (2).

204 $$\eta_{\mathrm{r}} = \left(1 - \frac{R_{\mathrm{cs},T,\mathrm{d}}}{R_{\mathrm{cs},T,\mathrm{u}}}\right) \times 100\% \quad (2)$$

205 where $R_{\mathrm{cs},T,\mathrm{u}}$ and $R_{\mathrm{cs},T,\mathrm{d}}$ are the temperature ranges upstream and downstream of the
206 mixer, respectively. The temperature range is defined as the difference between the maximum
207 and minimum temperatures measured in the cross-sectional temperature grid in each case.
208 While range effectiveness is useful for controlling mechanical systems, it is sensitive to
209 individual measurements and outliers. Therefore, statistical effectiveness, η_{s}, which offers
210 greater stability and robustness, is preferred when comparing the performance of different
211 mixing solutions. Statistical effectiveness is calculated using Eq. (3).

212 $$\eta_{\mathrm{s}} = \left(1 - \frac{\sigma_{\mathrm{cs},T,\mathrm{d}}}{\sigma_{\mathrm{cs},T,\mathrm{u}}}\right) \times 100\% \quad (3)$$

213 where $\sigma_{\mathrm{cs},T,\mathrm{u}}$ and $\sigma_{\mathrm{cs},T,\mathrm{d}}$ are the standard deviations in the temperature profiles
214 upstream and downstream of the mixer, respectively. In this paper, the temperature profile

downstream of the mixer is compared to the profile at the same location in the absence of the mixer. It is assumed that, in the absence of the mixer, the change in the temperature profile within the relatively short length of duct (60 mm) is negligible. Therefore, the profile measured without the mixer is considered representative of the upstream profile for comparison.

3. Results and discussion

In this section, the temperature profiles, mixing effectiveness, and pressure drops will be presented for various duct orientations and metal wool configurations with differing porosities and structures. A comparative analysis of these configurations is conducted to enhance understanding of metal wool air mixers and to support the selection of the most effective design.

3.1. Temperature profiles and mixing effectiveness

3.1.1. Horizontal orientation

The temperature profiles in the cross section of the duct in the horizontal orientation (a) before and (b) after adding the metal wool air mixer are shown in Figure 5. Without the mixer, there is a temperature gradient across the height of the duct, with lower temperatures at the bottom. The temperature range is 0.9°C, and the standard deviation of the temperature profile is 0.3°C. The temperature gradient from side to side is not as significant as was expected in this orientation. Adding the mixer homogenizes the temperature profile, reducing the temperature range to 0.3°C and the standard deviation to less than 0.1°C. The range effectiveness (η_r) and statistical effectiveness (η_s) of the mixer are 69% and 75%, respectively. It should be noted that effectiveness has been measured at 0.5 duct hydraulic diameter downstream of the mixer. Since mixing effectiveness increases with the distance downstream of mixers (Ahmed et al., 2020), the mixing effectiveness of the metal wool air mixer can be expected to be higher at farther distances downstream of the mixer. The

measured effectiveness of the bronze wool air mixer is comparable to conventional mixers such as louver mixers ($\eta_s \approx$ 75-85%) and orifice-target mixers ($\eta_s \approx$ 45-65%), evaluated at a downstream length of 1.5 hydraulic diameters (Ahmed et al., 2020).

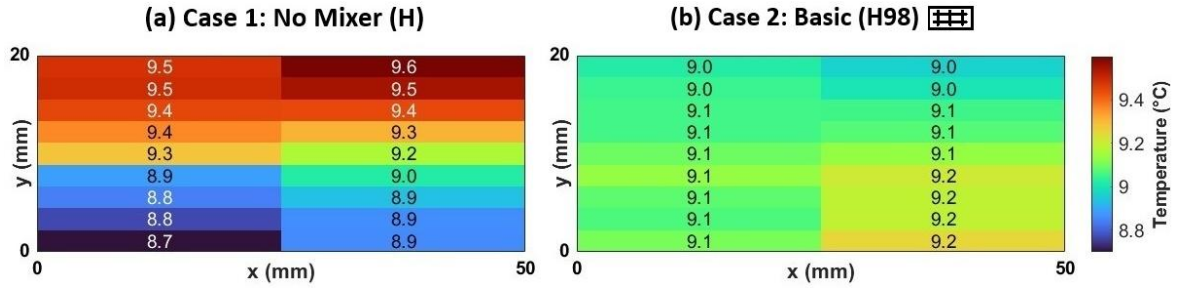

Figure 5. Temperature profiles in horizontal duct orientation: (a) Case 1 (no mixer); (b) Case 2 (ε = 98% & basic structure mixer).

3.1.2. Vertical orientation

Figure 6(a) shows the air flow pattern in the vertical duct downstream of the LAMEE, without the mixer. With the LAMEE oriented vertically, natural convection becomes significant. The cold membrane surface is located vertically on the left side, and the other three walls are insulated. Due to buoyancy forces, air descends near the cold membrane surface and rises near the opposite vertical wall to form a circulation flow pattern. Simultaneously, the fan-generated air flow occurs in the z direction, perpendicular to the plane of the duct cross-section (towards the observer).

Figure 6(b) to (f) present the temperature profiles in the vertical duct orientation for Cases 3 to 7 studied in this paper. In Figure 6(b), which shows Case 3 (No Mixer (V)), it is observed that without the mixer, the coldest location in the cross-sectional temperature grid is the bottom-left corner (nearest to the cold membrane surface) and the warmest location is the upper-right corner (furthest from the cold membrane surface). The temperature gradient in the vertical direction, with warmer air at the top and colder air at the bottom, is representative of the relatively significant natural convection expected in the vertical LAMEE orientation (Fauchoux et al., 2025). The temperature range is 1.5°C without the mixer, and the standard deviation of the temperature profile is 0.43°C.

In Case 4 (Basic (V99)), shown in Figure 6(c), adding the mixer with only 6.4 g of bronze wool reduces the temperature range to 1.0°C and the standard deviation to 0.21°C. The corresponding range effectiveness (η_r) and statistical effectiveness (η_s) of the mixer are 36% and 51%, respectively. In contrast, Case 5 (Directional (V97), shown in Figure 6(d)) uses a larger amount of bronze wool, resulting in a less porous structure; however, this does not improve mixing effectiveness over the lighter, more porous mixer in Case 4 (Basic (V99)). In this case, the temperature range is 1.3°C and the standard deviation is 0.41°C, resulting in a range effectiveness (η_r) of 15% and a statistical effectiveness (η_s) of 5%.

Although this observation may initially appear counter-intuitive, it can be explained based on the differences in the fibrous structure of the bronze wool in the two cases. In Case 4 (Basic (V99)), the metal fibers are randomly extended in all directions, promoting heat transfer both horizontally and vertically. In Case 5 (Directional (V97)), the increased amount of bronze wool is compressed to fit in the limited space of the cassette, causing the fibers to align predominantly in the vertical (y) direction. This rearrangement enhances heat conduction in the vertical (y) direction at the expense of horizontal (x-direction) heat conduction. This explanation is supported by gradients in the temperature profile of Case 5, where the vertical temperature ranges (at fixed distances along the x-axis) are significantly lower than the horizontal temperature ranges (at fixed distances along the y-axis). Although the duct is narrower in the horizontal direction, the mixer in Case 5 is less effective in eliminating the horizontal temperature gradients due to the directional orientation of the wool structure.

Figure 6(e) shows Case 6 (Spiral (V97)), with a wool mass and porosity identical to Case 5 (Directional (V97)) but a different wool structure (spiral). The different wool structure is introduced to improve the effectiveness of the mixer and further investigate the explanation provided above. The temperature range in Case 6 is 1.2°C and the standard deviation is

0.36°C, resulting in a range effectiveness of 22% and a statistical effectiveness of 16%. These values represent an improvement over Case 5. While the increase in range effectiveness falls within the measurement uncertainty, the improvement in statistical effectiveness is significant. This enhanced performance from Case 5 to Case 6 confirms the detrimental effect of the directional orientation of metal wool fibers on the effectiveness of the air mixer.

Figure 6(f) shows Case 7 (Accordion (V97)), with accordion wool structure and a wool mass and porosity identical to Case 5 (Directional (V97)) and Case 6 (Spiral (V97)). In this case, the range and statistical effectiveness values are 54% and 44%, respectively. The accordion wool structure used in Case 7 exhibits significantly higher range and statistical effectiveness than the directional and spiral structures used in Cases 5 and 6. The observed improvement is attributed to a more uniform flow distribution and an enhanced fibrous structure that facilitates multi-directional heat conduction.

Despite the 18% increase in range effectiveness and the 7% decrease in statistical effectiveness from Case 4 (Basic (V99)) to Case 7 (Accordion (V97)), a confident comparison between these two top-performing cases is not possible because their performances overlap within the bounds of measurement uncertainty. Even so, the differences are examined as potentially meaningful to explore the possible influence of wool structure on mixer performance. The 7% reduction in statistical effectiveness can be attributed to greater temperature dispersion observed in Case 7, particularly in the upper half of the duct. The increased temperature dispersion is likely due to the compactness of the wool, which restricts advection and mechanical mixing across the duct cross-section. A metal wool air mixer that combines the structural benefit of the accordion form of Case 7 with the higher porosity of Case 4 may offer improved performance in terms of statistical effectiveness.

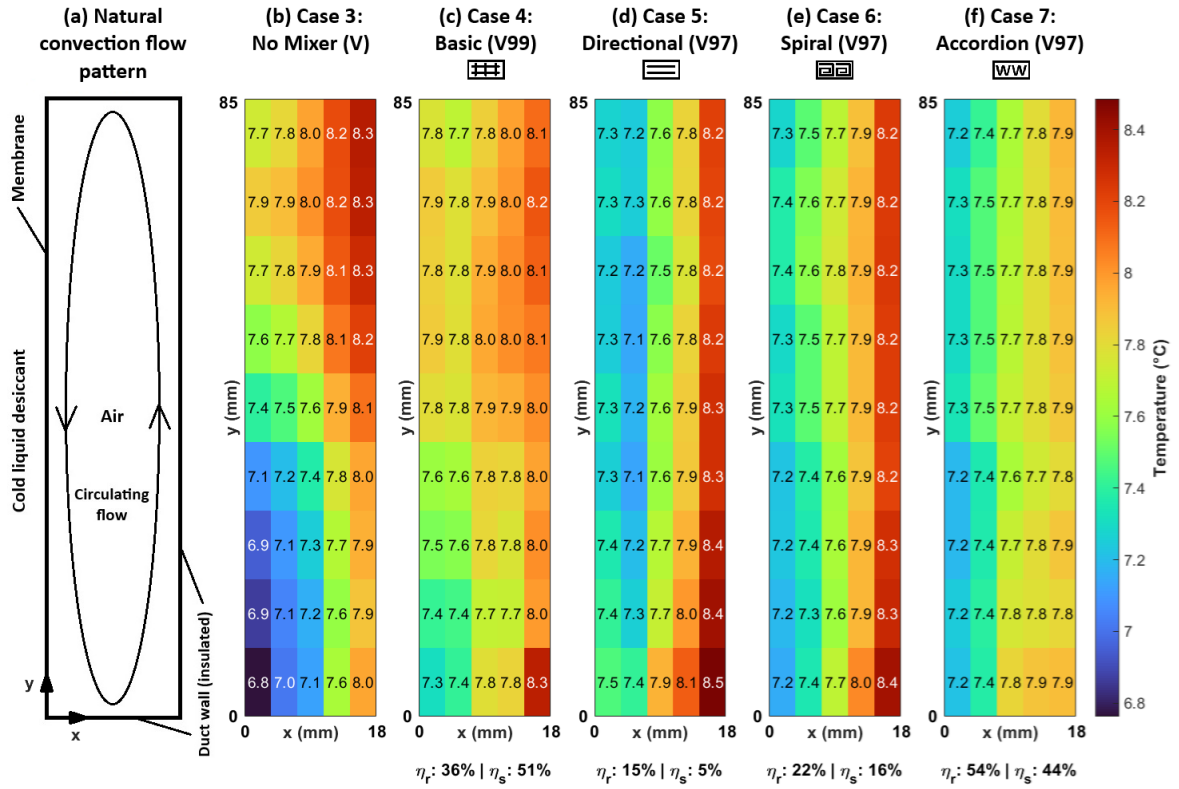

Figure 6. Air flow pattern and temp profiles in vertical orientation: (a) Flow pattern in the absence of the mixer; and the temperature profiles in (b) Case 3 (no mixer); (c) Case 4 (ε = 99% & basic structure); (d) Case 5 (ε = 97% & directional structure); (e) Case 6 (ε = 97% & spiral structure); (f) Case 7 (ε = 97% & accordion structure).

Table 6 summarizes the range and standard deviation of the temperature profiles, along with the range effectiveness and statistical effectiveness of the mixers in each case. The ranges of statistical effectiveness reported by Ahmed et al. (2020) for two common types of conventional air mixers, i.e. louver and orifice-plate air mixers, are also added to the table for comparison. The measured performance of Case 2 (Basic (H98)), Case 4 (Basic (V99)), and Case 7 (Accordion (V97)) in this study is comparable to that of the conventional mixers.

Table 6. Summary of the results: the range and standard deviation of the temperature profiles, the range effectiveness, and the statistical effectiveness of the mixer in each case. Two examples of conventional mixer performance values are also provided for comparison.

Case #	Range, $R_{cs,T}$ (°C)	Standard deviation, $\sigma_{cs,T}$ (°C)	Range effectiveness, η_r (%)	Statistical effectiveness, η_s (%)
1	0.90	0.30	-	-
2	0.28	0.08	69	75
3	1.5	0.43	-	-
4	1.0	0.21	36	51
5	1.3	0.41	15	5
6	1.2	0.36	22	16
7	0.73	0.24	54	44
Statistical effectiveness of conventional mixers (for comparison), η_s (%) (Ahmed et al., 2020)				
Louver mixer				75-85
Orifice-target mixer				45-65

3.2. Mechanisms of temperature homogenization

With metal wool air mixers, physical mixing may result from flow agitation induced by the metal fibers and variations in local flow velocities around them (Figure 7(a)). This mechanism, resembling the diffusive mixing process proposed by Heijnen and Van't Riet (1984) for liquid mixing in bubble columns, is expected to have a comparatively minor effect on mixing and temperature homogenization. When the porosity of the medium is sufficiently high to form relatively large open spaces within the wool structure, a secondary mixing process may occur, involving the formation of small eddies behind the fibers and localized recirculation within the interstitial regions (Figure 7(b)). However, due to the low Reynolds numbers in this study, mechanical dispersion is expected to be limited, as Basilio et al. (2023) suggest that such mechanisms become more prominent at higher Reynolds numbers.

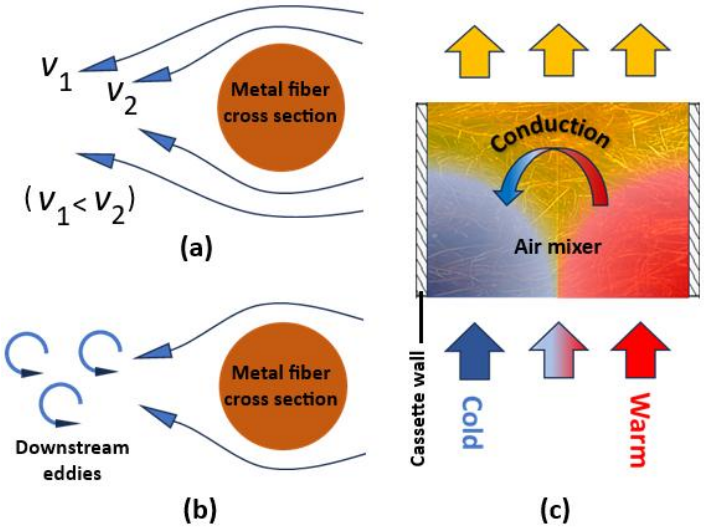

Figure 7. Temperature homogenization mechanisms in the bronze wool air mixer, including (a) the diffusive mixing mechanism due to velocity gradients near the fibers, (b) formation of eddies behind the fibers, and (c) thermal conduction through the metal fibers.

While mechanical mixing is limited under the operating conditions of this study, heat conduction is likely the dominant contributor to the observed uniform temperature profiles, particularly in configurations with more compact metal wool structures. The high thermal conductivity of the metal fibers helps reduce temperature gradients as air flows through the mixer. Under steady-state conditions, the metal fibers absorb heat from warmer regions of the air stream and transfer it to cooler regions via conduction (Figure 7(c)). This mechanism enables the proposed metal wool air mixer to maintain effective temperature homogenization even when the porous structure or flow conditions do not permit significant mechanical mixing. Although the suggested mechanisms require further validation through experimental or theoretical investigation, they provide a plausible explanation for the results observed in this study.

3.2.1. Pressure drop

The pressure drops across the mixer were measured for Cases 2 (Basic (H98)), Case 4 (Basic (V99)), Case 5 (Directional (V97)), and Case 7 (Accordion (V97)) over a range of Reynolds numbers, and the results are presented in Figure 8. Case 7 is not shown in Figure 8 because the pressure drops in Case 7 are similar to Case 5 within the uncertainty of

measurements, which could be expected due to the identical porosities of the metal wool in the two cases.

In Case 2 (Basic (H98)), flow rates range from 2.0 to 30.0 LPM, corresponding to Reynolds numbers between 39 and 586. As expected, the pressure drop increases with Reynolds number. At Re = 39, the pressure drop is 2.8 Pa and increases to 14.3 Pa at Re = 360, and 23.5 Pa at Re = 586. In Case 5 (Directional (V97)), flow rates range from 5.5 to 19.5 LPM, corresponding to Reynolds numbers between 100 and 360. The pressure drop is 4 Pa at Re = 100, and increases to 21 Pa at Re = 360. The higher pressure drops in Case 5 (Directional (V97)) compared to Case 2 (Basic (H98)) are due to the lower porosity in Case 5. Case 4 (Basic (V99)), which has the highest porosity (ε = 99%), exhibits the lowest pressure drops. While the expected increasing trend with Reynolds number is observed for this case, the minor variations between data points fall within the measurement uncertainty. The highest pressure drop observed in this case is 3.6 Pa.

Under the low Reynolds numbers considered in this study, the pressure loss induced by the mixer remained relatively small compared to other components, such as the orifice plates, which produced losses in the range of 300 to 3500 Pa. The relationship between pressure drop and Reynolds number follows a linear trend. The regression correlation and the coefficient of determination are provided on the graph for each case in Figure 8.

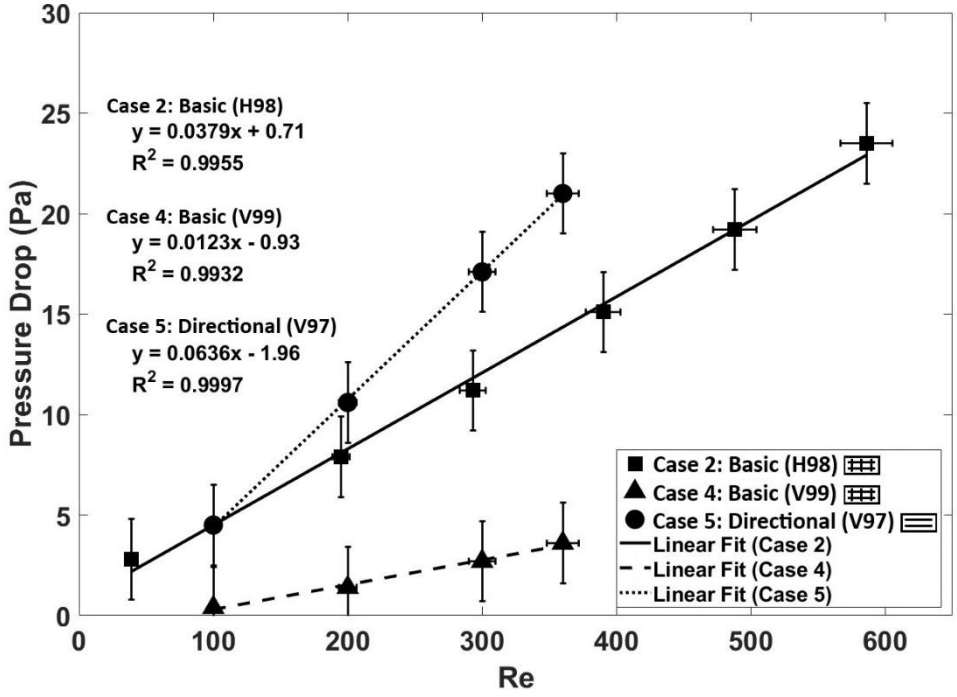

Figure 8. Pressure drops caused by the bronze wool air mixer at different air Reynolds numbers in Case 2 (ε = 98%, basic structure, horizontal), Case 4 (ε = 99%, basic structure, vertical), and Case 5 (ε = 97%, directional structure, vertical). The lines represent the results of linear regression over the experimental data in each case. The regression correlation and the coefficient of determination are also provided for each case.

4. Conclusion

This study investigated the use of metal wool to homogenize the air temperature distribution in duct systems, an application that has not been previously explored. The thermal mixing performance of a bronze wool air mixer inserted into an air duct was evaluated experimentally. The goal was to achieve a uniform temperature profile in the air outlet of a liquid-to-air membrane energy exchanger (LAMEE). Different orientations of the duct (and LAMEE), as well as different bronze wool porosity and structures, were studied. Measurements included temperature profile and pressure drop caused by the mixer. The main findings are summarized below.

- The application of bronze wool as an air mixer significantly improved temperature uniformity. In the horizontal orientation (Case 2: Basic (H98)), the temperature range was decreased from 0.9°C to 0.3°C, and the standard deviation dropped to less than 0.1°C when the mixer was used. The range effectiveness and statistical

mixing effectiveness of the mixer were 69% and 75%, respectively. These values are comparable with traditional mixers such as louvers and orifice-targets.

- The suggested dominant temperature homogenization mechanism in metal wool air mixers under low Reynolds number and high wool compactness conditions is thermal conduction through the metal fibers. While mechanical mixing due to flow agitation and recirculation is minimal under such conditions, the metal fibers transfer heat from the warmer to the colder spots of the air flow and effectively reduce temperature gradients in the air stream.
- In the vertical orientation, air mixers with different masses and wool structures were tested. The range effectiveness and statistical effectiveness of the mixer decreased from 35% and 51% for the lighter, more porous mixer in Case 4: Basic (V99) (m = 6.4 g, ε = 99%) to 15% and 5% for the heavier, less porous mixer in Case 5: Directional (V97) (m = 23.4 g, ε = 97%). Despite the increase in the wool mass and compactness in Case 5, the thermal mixing effectiveness decreased because the metal fibers were arranged mainly in the vertical direction.
- It is suggested that the conduction heat rate is stronger in the direction along which most of the metal fibers are aligned. Therefore, a mixer with fibers predominantly oriented along a specific direction fails to eliminate the temperature gradients in other directions. A comparison of the two mixers in Cases 5: Directional (V97) and Case 6: Spiral (V97), which have the same wool mass and porosity but different wool structures, supports this explanation. The mixer with the spiral wool structure (Case 6) had a range effectiveness of 22% and a statistical effectiveness of 16%. These values show an improvement in mixing effectiveness over the mixer with vertically aligned fibers (Case 5).

- The accordion wool structure in Case 7 (Accordion (V97)) achieves a higher range effectiveness (54%) and statistical effectiveness (44%) than Case 5 (Directional (V97)) and Case 6 (Spiral (V97)), with the same wool mass and porosity. This improvement is attributed to improved flow uniformity and multi-directional heat conduction enabled by the enhanced fibrous structure in Case 7.
- The accordion wool structure in Case 7 (Accordion (V97)) increases range effectiveness by 18% but decreases statistical effectiveness by 6%, compared to the basic wool structure in Case 4 (Basic (V99)). These changes in performance fall within the bounds of measurement uncertainty, which makes a confident comparison between these two top-performing cases impossible. Assuming that the decrease in statistical effectiveness is meaningful, it can be attributed to reduced physical mixing in the more compact wool structure of Case 7.
- The uncertainty in evaluating range effectiveness is relatively high in this study, primarily due to the limited temperature range observed under the tested operating conditions. These conditions were chosen to reflect the typical operating scenario of the experimental research that motivated this work. However, the temperature range, and consequently the uncertainty in range effectiveness, could be improved by operating the energy exchanger upstream of the mixer at higher temperature differences.
- The pressure drop was measured at various Reynolds numbers for mixers with different orientations and porosities. At a given Reynolds number, the least porous (most compact) metal wool air mixer (Case 5: Directional (V97)) produces the highest pressure drop. For instance, at Re = 350, a 20 Pa pressure drop was measured for this case. Nonetheless, the pressure drops caused by the bronze wool air mixer in all cases studied in this paper were generally insignificant compared

to the other sources of pressure loss in the system, such as the orifice plates, which caused pressure drops between 300 and 3500 Pa.

This research presents metal wool air mixers as a viable, effective solution for achieving temperature homogeneity, especially in small-scale and laboratory applications, where installation flexibility and low space requirements are necessary.

5. Future work

The experimental work presented in this study provides a foundation for the application of metal wool as an effective air mixer when the mixer is used to homogenize the temperature profile. Future research can build on this by addressing the following areas:

- Other wool structures: Testing the performance of mixers with other metal wool structures and porosities to identify configurations that further optimize thermal mixing effectiveness while minimizing pressure drop.
- Establishing a methodology for sizing metal wool air mixers: an extensive study on the relationship between mixing effectiveness, and the dimensions of the mixer for metal wools of different porosities and thermal conductivities can result in a method to determine the appropriate mixer size for any given application.
- Analysis of mixing mechanisms: Further investigations, especially computational studies, can clarify the internal flow behavior within the porous metal wool structure, including the formation of eddies and recirculation, and assess how mixing mechanisms vary with porosity.

Declaration of competing interests

The authors declare there are no competing interests.

Data availability

Data will be made available upon request.

References

Ahmed, M., Park, H., Bach, C.K., San, O., 2020. Numerical investigation of air mixer for HVAC testing applications (ASHRAE RP-1733). Sci Technol Built Environ 26, 1252–1273. https://doi.org/10.1080/23744731.2020.1793617

ASHRAE, 2020. ANSI/ASHRAE standard 84-2020: methods of testing air-to-air heat/energy exchangers. Atlanta.

ASME, 2019. ASME PTC 19.1-2018: Test uncertainty. New York.

ASTM, 2020. ASTM E104-20a: Standard practice for maintaining constant relative humidity by means of aqueous solutions. https://doi.org/10.1520/E0104-20A

Basilio Hazas, M., Ziliotto, F., Lee, J., Rolle, M., Chiogna, G., 2023. Evolution of plume geometry, dilution and reactive mixing in porous media under highly transient flow fields at the surface water-groundwater interface. J Contam Hydrol 258. https://doi.org/10.1016/j.jconhyd.2023.104243

Bergman, Lavine, Incropera, Dewitt, 2017. Fundamentals of heat and mass transfer, Eighth. ed. Wiley, Hoboken.

Faison, T.K., Davis, J.C., Achenbach, P.R., 1970. Performance of Louvered Devices as Air Mixers.

Faison, T.K., Davis, J.C., Achenbach, P.R., 1967. Performance of square-edged orifices and orifice-target combinations as air mixers. National Bureau of Standards, U.S. Department of Commerce, Washington, D.C.

Fauchoux, M.T., Mahmoudi, A., Gollamudi, S., Niroomand, S., Navid, P., Joseph, A., Simonson, C.J., 2025. Frosting on porous membranes in energy exchangers. Philosophical Transactions of the Royal Society A. https://doi.org/10.1098/rsta.2024.0365

Heijnen, J.J., Van't Riet, K., 1984. Mass transfer, mixing and heat transfer phenomena in low viscosity bubble column reactors. Chemical Engineering 28, B21–B42.

ISO, 2003. ISO 5167-2:2003 Measurement of fluid flow by means of pressure differential devices inserted in circular-cross section conduits running full - Part 2: Orifice Plates.

Li, B., Xu, H., Song, Y.J., Zhang, H.L., Wang, W.W., Zhao, F.Y., 2023. Heat and moisture transports in a slot ventilated enclosure packed with discrete porous media: Mixing convection instability, oscillation and resonance. International Journal of Thermal Sciences 194, 108603. https://doi.org/10.1016/j.ijthermalsci.2023.108603

Reader-Harris, M., 2015. Orifice plates and venturi tubes, 1st ed. Springer, Glasgow. https://doi.org/10.1007/978-3-319-16880-7 ISSN

Robinson, K.D., 1997. Static air mixer fundamentals. Heating, Piping, and Air Conditioning (HPAC) 85–90.

Rousseau, G., Izumoto, S., Le Borgne, T., Heyman, J., 2023. Dispersion Versus Diffusion in Mixing Fronts. Water Resour Res 59, 1–14. https://doi.org/10.1029/2023WR035848